Structural Sizing of a Composite Transonic Truss-Braced Wing

Erin K. Anderson*, Alana M. Cardona*, and Brian H. Mason‡
NASA Langley Research Center, Hampton, VA 23681-2199

Accurate finite element modeling (FEM) is a vital part of the modern aircraft design process. As aircraft become increasingly complex, the time-consuming nature of detailed FEM approaches comes at a significant cost to program timeline and budget. In an effort produce modeling efforts that are sufficiently accurate and minimally costly, a proposed FEM approach and optimization scheme for a composite aircraft is explored, including a discussion of the manufacturing constraints of a highly tailored composite panel design. A high-fidelity structural model of a transonic truss-braced wing (TTBW) is generated, and the components are sized by structural optimization to satisfy buckling and strength constraints while subjected to critical maneuver loads. The structural modeling approaches and sizing of a TTBW are discussed, including details for FEM approaches, verification of an approximated FEM approach, a sizing optimization using the optimization software LS-OPT, and a manufacturing trial of integrally stiffened composite panels conducted to explore the validity of highly tailored composites as a design consideration. The results of study discussed herein indicate that the proposed FEM approach is suitable for modeling composite-construction aircraft and for use in sizing optimization. Further efforts regarding integrally stiffened composite panels will indicate the suitability of this method for the integration of highly tailored composite panels into the design and optimization process, given the manufacturability of such panels as shown here.

I. Introduction

The NASA Advanced Air Transport Technology (AATT) project is tasked with drastically reducing fuel consumption, noise, and emissions in the next generation of aircraft, with a focus on subsonic fixed-wing commercial transports. One promising technology that AATT is considering is the use of an ultra-efficient transonic truss braced wing (TTBW). One TTBW concept under consideration is the subsonic ultra-green aircraft research (SUGAR) concept, which is designed to operate efficiently at a cruise speed of Mach 0.75 [1].

The SUGAR design is predicted to give a 5%-7% reduction in fuel consumption compared to traditional tube and cantilever wing single-aisle transport aircraft [1]. Critical to the success of SUGAR and other TTBW designs is a process to create an efficient, low-weight structural design. To date, the testing program for TTBW concepts at NASA has primarily been focused on aerodynamic and aeroelastic performance [2, 3] or used low-fidelity structural models [4, 5]. Structural testing will be needed to ensure that the low-weight structural designs based on current analyses are able to support these aerodynamic load cases.

External struts have not traditionally been used to reinforce the wings of transonic aircraft. Therefore, accurate structural modeling and design of aircraft structural joints, especially truss joints, is necessary to properly evaluate the performance of a TTBW concept. The proposed SUGAR aircraft concept is shown in Figure 1, and includes both a main strut, highlighted in red, and a smaller jury strut, highlighted in yellow. Detailed structural data, such as skin thickness and wing stiffness, are rarely available from airframe manufacturers, but planform data, such as for the Phase III SUGAR concept, are publicly available. [1]

* Research Aerospace Engineer, Structural Mechanics and Concepts Branch, Mail Stop 190, AIAA Member
‡ Research Aerospace Engineer, Structural Mechanics and Concepts Branch, Mail Stop 190, AIAA Associate Fellow.

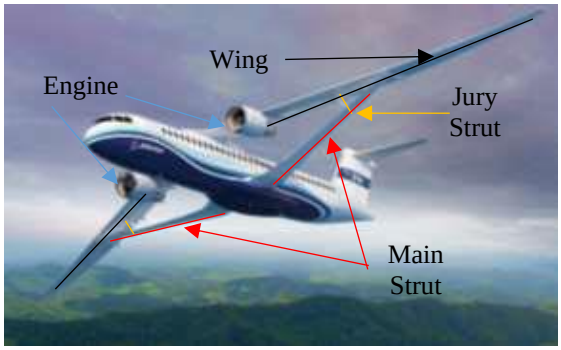

Figure 1. A proposed TTBW aircraft concept.

In this paper, discussed is the generation of a high-fidelity structural model in which the components are sized by structural optimization to satisfy buckling and strength constraints while subject to critical maneuver loads. The structural modeling approaches and sizing of a TTBW are discussed in the following manner: details for the finite element model (FEM) approaches will be discussed for the full-wing configuration first; second, an approximated FEM approach will be described; third, a composite laminate sizing optimization will be considered; then, an integrally stiffened strut configuration will be discussed; and finally, concluding remarks and forward work will be provided.

II. FEM of a Transonic Truss-Braced Wing

Finite element (FE) analysis is the preferred technique for computational simulation of structural responses. Unfortunately, generation of a complete airframe FEM is typically a labor-intensive process. An automated mesh-generation tool called the Conceptual Design Shop (CDS) was used to facilitate creation of a FEM of the wing [6], while the truss structures were created manually using the MSC/PATRAN[1] [7] FE modeling tool. Stress and buckling analyses were performed using the general-purpose FE code MSC/NASTRAN [8].

The FEM of the TTBW consisted of 16,935 shell (quadrilateral and triangular) elements, 807 beam elements, 66 point masses, and 15,322 nodes and is illustrated in Figure 2 where the complete FEM boundary conditions are illustrated in Figure 2a and the wing and truss covers are removed to show the spars and ribs in Figure 2b. The distributed loads shown in Figure 2b sum to half the gross-takeoff weight of the aircraft. Load scenarios include a -1-g down gust load case and a +2.5-g climb load case. For the initial FEM, multi-point constraints were used to connect the main and jury struts to the rest of the wing structure. All modeling approaches discussed in this paper were considered with the goal of selecting efficient, appropriate modeling methods to be used in a full, global wing structure model.

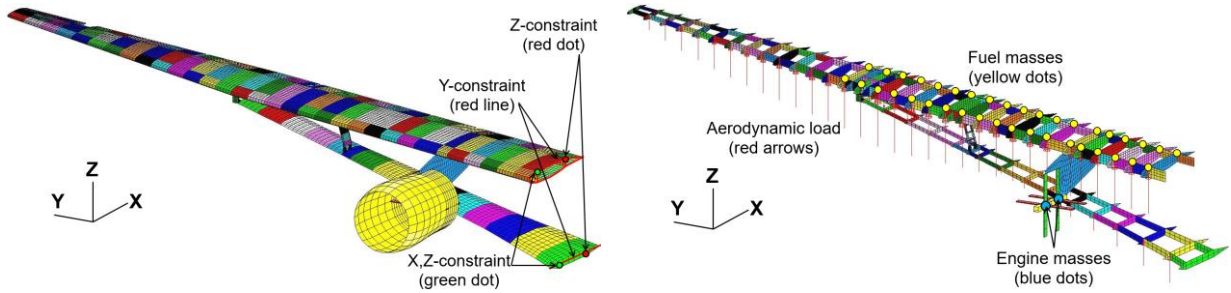

(a) FEM of wing, main strut and jury strut, and engine nacelle

(b) FEM with covers removed for visibility of internal structures

Figure 2. Global TTBW FEM.

[1] The use of trademarks or names of manufacturers in this report is for accurate reporting and does not constitute an official endorsement, either expressed or implied, of such products or manufacturers by the National Aeronautics and Space Administration.

The wing was divided into 32 bays; each bay was bounded by a forward spar, an aft spar, and two ribs. In the global model, control surfaces were fully connected to the aft spar. Similarly, the main strut and jury strut were divided into 15 bays and 4 bays, respectively. The wing and struts were composed of composite laminates of the common carbon-epoxy material system IM7/8552 [9], with the material properties given in Table 1. Stacking sequences for the wing and struts were determined by a sizing process described in Section V. The engine mount and nacelle were given aluminum properties provided in Table 1. The engine and nacelle were included only to provide a load path for the engine weight; hence, these components were defined with zero mass and the thicknesses were not sized. The engine and nacelle masses were represented by two point-masses located at the engine center of gravity (CG) location and were connected to the nacelle with beam elements.

The wing planform had a surface area of 212,600 sq. in. (total for both right and left wings) with an aspect ratio of 19.6. The trapezoidal wing tapered 88% at the 58% spanwise location where the main strut intersected the wing. The taper ratio at the tip was 35%. The airfoil section was similar to the Boeing model described in Reference [1].

Table 1. Material properties.

Property	IM7/8552 [9]	Aluminum
Weight density, lbf/in.^{3}	0.05714	0.100
Elastic Modulus – Longitudinal, Msi	22.99	10.60
Elastic Modulus – Transverse, Msi	1.30	10.60
Shear Modulus, Msi	0.68	3.98
Poisson's Ratio	0.316	0.330
Tensile Strength – Longitudinal, ksi	362.69	N/A
Tensile Strength – Transverse, ksi	9.29	N/A
Compressive Strength – Longitudinal, ksi	-248.94	N/A
Compressive Strength – Transverse, ksi	-41.44	N/A
Shear Strength, ksi	13.22	N/A

III. Finite Element Modeling to Approximate Stiffened Wing Panels

Creating a detailed FEM with stiffeners individually modeled as beam elements is a common approach for detailed analysis of stiffened panels. In this paper, an alternative to this approach was proposed, wherein the same wing geometry was modeled with a composite ply layer in lieu of beam elements. This composite smeared layer (CSL) was assigned smeared bulk properties scaled volumetrically to result in the same stiffening properties as the traditional FEM with beam-element stiffeners. This approach is attractive as it is less labor intensive to modify one composite layer than many discrete beam elements, increasingly so if design changes drive frequent modifications to the FEM mesh.

For this study, two geometries, a rectangular panel and a trapezoidal panel, were constructed and the respective models were identically loaded to compare the discrete-beam and CSL modeling approaches. A third modeling approach, named the hybrid model, was explored employing the CSL model with additional edge beam stiffeners at the extreme edges of the model to further reduce discrepancy between the beam-reinforced baseline and the proposed CSL approach. An approximation of the sideview of a panel element and beam stiffener and its CSL stiffener equivalent, labeled Ply Stiffener, are shown in Figure 3. An approximation of the hybrid-beam and CSL model is shown in Figure 4. In the CSL approach, a new composite layer with its own material property is appended to the existing composite layup. The density, shear moduli, and elastic modulus in the beam axial direction associated with this layer are scaled by a volumetric fraction. The volumetric fraction is the ratio of the thickness of the beam stiffener to the stiffener spacing. The elastic moduli in the axes of the beam cross-section are set to a low value (1.0 psi).

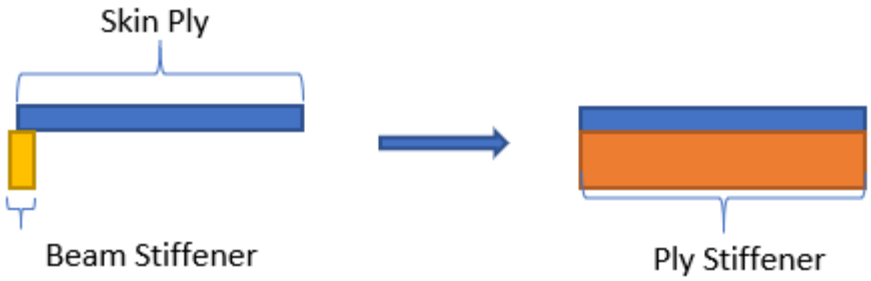

Figure 3. Panel element stiffened by a beam element and its equivalent with a CSL ply stiffener.

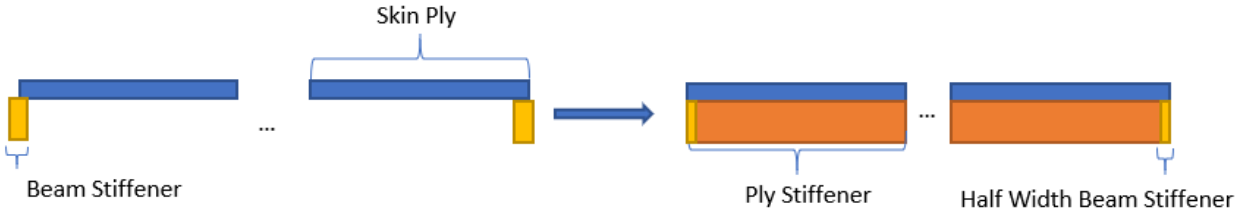

Figure 4. Panel edge elements with a beam stiffeners and equivalent with hybrid CSL ply stiffeners and half-width beam stiffeners.

The rectangular panel geometry is shown in Figure 5; this geometry is the simplest geometry case considered because it is meshed such that all shell elements are of the same size and evenly spaced. In contrast, the trapezoidal panel geometry, where the real-world design necessitates evenly spaced stiffeners, requires either a FEM with both triangular and rectangular elements (Figure 6a) or a FEM with stiffeners placed at uneven intervals (Figure 6b). A CSL approach allows more freedom in mesh design, as the need for discrete stiffeners placed at regular intervals is eliminated.

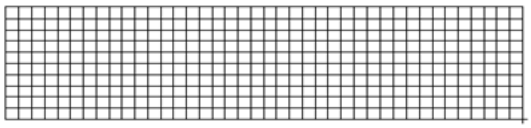

Figure 5. Rectangular panel geometry.

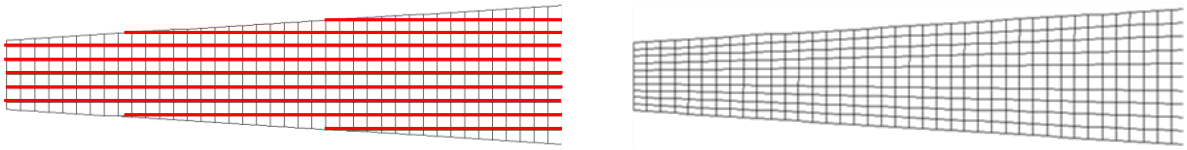

(a) FEM accommodating beam spacing (beams shown in red)

(b) FEM without accommodating beam spacing

Figure 6. Tapered trapezoidal panel models.

For both geometries, a beam-reinforced model was used to establish a baseline for maximum displacement and Tsai-Hill failure index. Aluminum blade stiffeners that were 0.5-in. high, and 0.1-in. thick with a 5-in. spacing were added to the mesh in Figure 5. The same geometry was used to create a model consisting of only composite shell elements, with an added CSL replacing the beam stiffeners. Aluminum material properties Young's modulus (E), shear modulus (G), and density (ρ) scaled to a volumetric fraction of 2% were assigned to the CSL ply layer. All models were cantilevered and clamped at the root, with a 250-lb. distributed load applied across the tip edge and assessed at a 1.0 factor of safety. A reduction in stiffness associated with the scaling of the shear modulus was observed for both geometries. To increase the CSL model stiffness to that of the baseline model, half-width beam stiffeners were placed on the edges of both CSL models. Preliminary Tsai-Hill failure index results are plotted as contours and

displacements are shown relative to the unloaded model in Figure 7 and Figure 8 for the rectangular panel geometry and the trapezoidal panel geometry, respectively. The tabulated displacements and failure indices for these models are shown in Table 2. The CSL model displacement results are within 4% of the baseline displacement results and the failure index results are within 3% of the baseline results for both geometries. The hybrid models show closer correlation, reducing the discrepancies with the baseline models to within 2% for both displacement and failure index results.

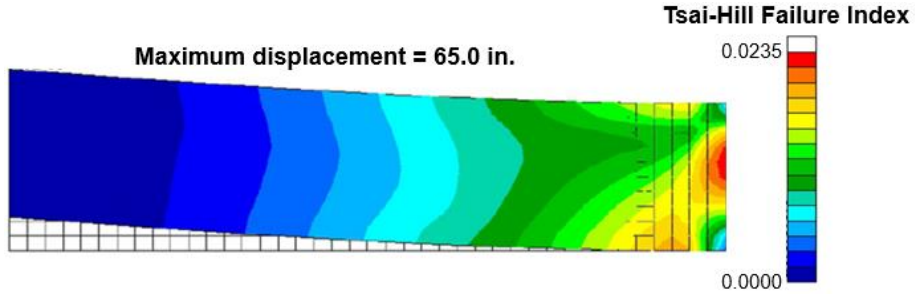

(a) Beam-reinforced FEM results

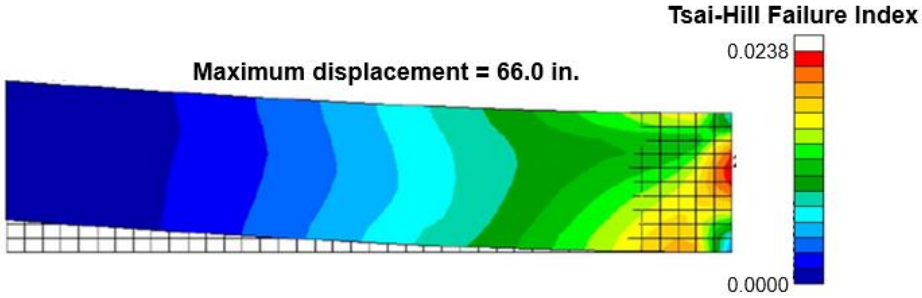

(b) CSL-reinforced FEM results with E, G, and ρ stiffener properties scaled volumetrically

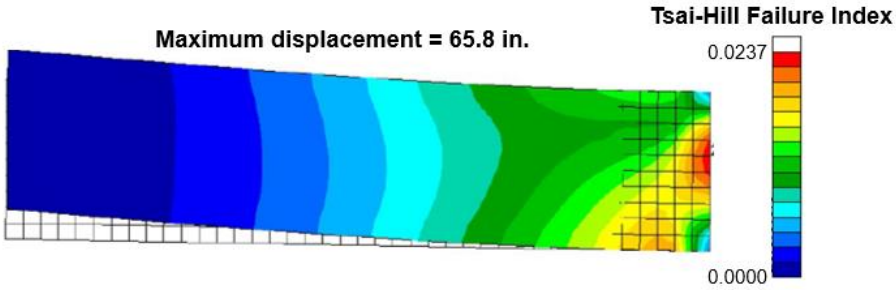

(c) Hybrid beam- and CSL-reinforced (E, G, and ρ scaled) FEM results

Figure 7. Tsai-Hill failure and displacement results for rectangular panel FEM.

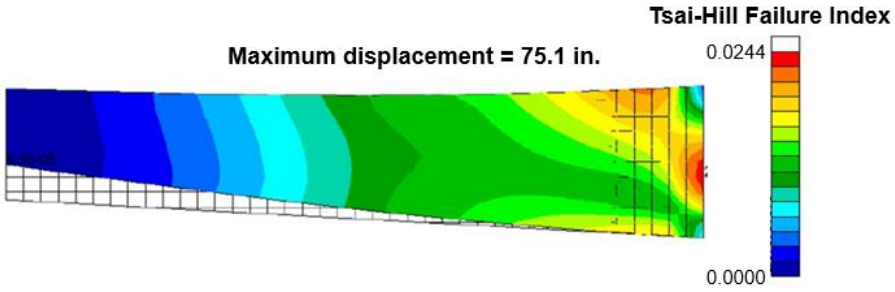

(a) Beam-reinforced FEM results

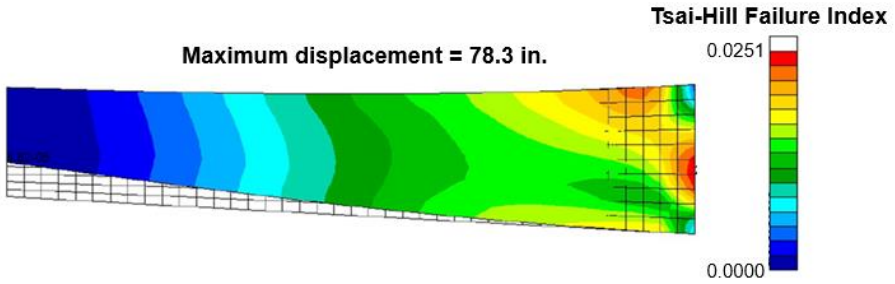

(b) CSL-reinforced FEM results with E, G, and ρ stiffener properties scaled volumetrically

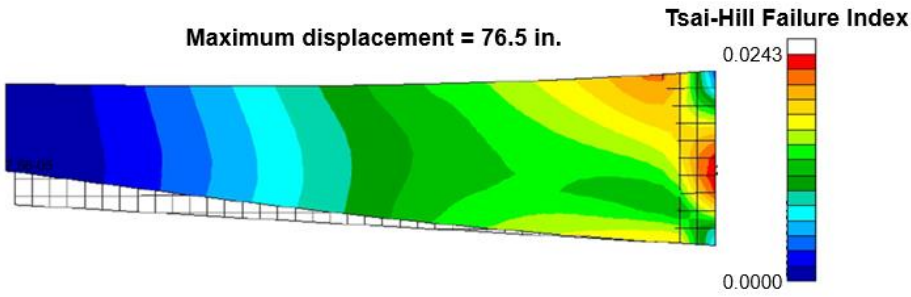

(c) Hybrid beam- and CSL-reinforced (E, G, and ρ scaled) FEM results

Figure 8. Finite Element Tsai-Hill failure and displacement results for trapezoidal panel model.

Table 2. Tabulated displacement and Tsai-Hill failure indices for approximated stiffener FEM approaches

Model	Maximum Displacement, in.	Displacement Difference to Beam Baseline, %	Maximum Tsai-Hill Failure Index	Failure Index Difference to Beam Baseline, %
Rectangular Panel Beam-Reinforced	65.0	-	0.0235	-
Rectangular Panel CSL-Reinforced	66.0	+1.54	0.0238	+1.28
Rectangular Panel Hybrid Beam- and CSL-Reinforced	65.8	+1.23	0.0237	+0.85
Trapezoidal Panel Beam-Reinforced	75.1	-	0.0244	-
Trapezoidal Panel CSL-Reinforced	78.3	+3.99	0.0251	+2.87
Trapezoidal Panel Hybrid Beam- and CSL- Reinforced	76.5	+1.86	0.0243	-1.64

IV. Integration into Global TTBW FEM

Given the high level of correlation between the CSL-reinforced modeling methods and the beam-reinforced baseline models, the CSL-reinforced and hybrid-reinforced methods were applied to the global TTBW FEM as discussed in Section II. To establish a baseline for comparison, beam elements were added to the section of the unreinforced wing model as shown in Figure 9. These beam elements were defined as aluminum blade stiffeners that were 1.5-in. high, and 0.15-in. thick and with a 5-in. spacing.

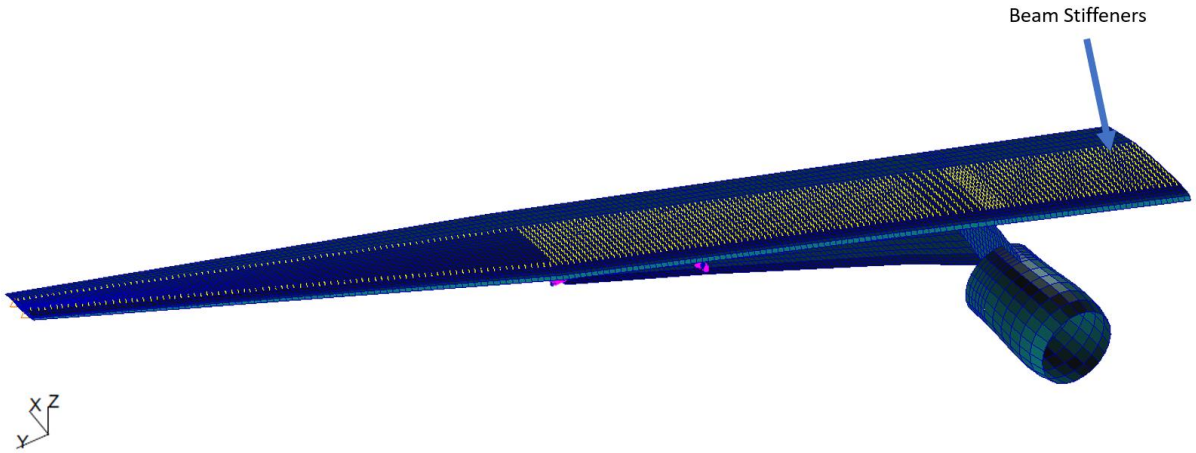

Figure 9. Global TTBW FEM with beam stiffener locations in yellow.

As shown in Figure 10, a composite layer was added to the composite shell elements corresponding to the beam element stiffener locations in the beam-reinforced model. This composite layer was assigned a material property with E, G and ρ of the beam element material weighted by the volumetric dimension change between the beam elements and the smeared layer. Finally, a hybrid model was developed using the CSL from the previous model and the edge beam elements from the beam-reinforced model. Both the beam-reinforced locations and the CSL element locations are shown in Figure 11.

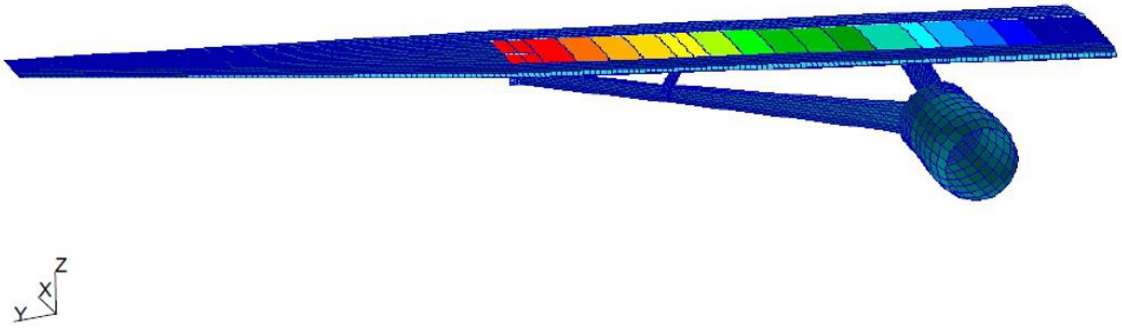

Figure 10. Global TTBW FEM with CSL stiffener property set indicated by color.

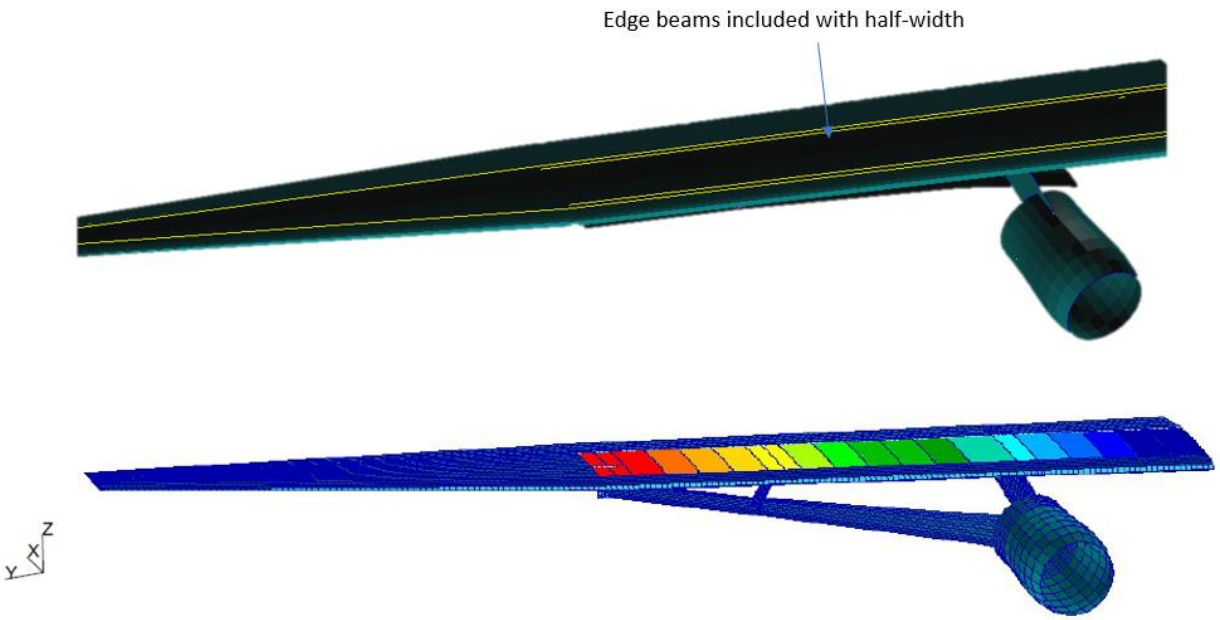

Figure 11. Global TTBW FEM with hybrid model beam and CSL element locations.

All models were run using the NASTRAN linear solution SOL 101 under the +2.5-g climb loading conditions discussed in Section II with a 1.0 factor of safety. Results for maximum displacement and failure index of the shell composite elements (excluding CSL, where present) were compared with the unreinforced model to ensure anticipated model behavior, and with the beam-reinforced baseline model to confirm equivalent modeling results. Results are tabulated in Table 3. The maximum displacement (in true scale) and failure index (plotted as a spectrum for each model) for the +2.5-g climb load case are shown in Figure 12 through Figure 15. Note that the model is flipped upside down in these figures to more clearly display the location of the maximum failure index. Maximum displacement occurs at the wing tip in all models.

Table 3. Tabulated displacement and Tsai-Hill failure indices for approximated stiffener FEM approaches in global model

Global TTBW Model Version	Maximum Displacement, in.	Displacement Difference to Beam Baseline, %	Maximum Tsai-Hill Failure Index	Failure Index Difference to Beam Baseline, %
Unreinforced	28.1	-	0.252	-
Beam-Reinforced	27.6	-	0.185	-
CSL-Reinforced	27.5	-0.36	0.192	+3.78
Hybrid-Reinforced	27.5	-0.36	0.190	+2.70

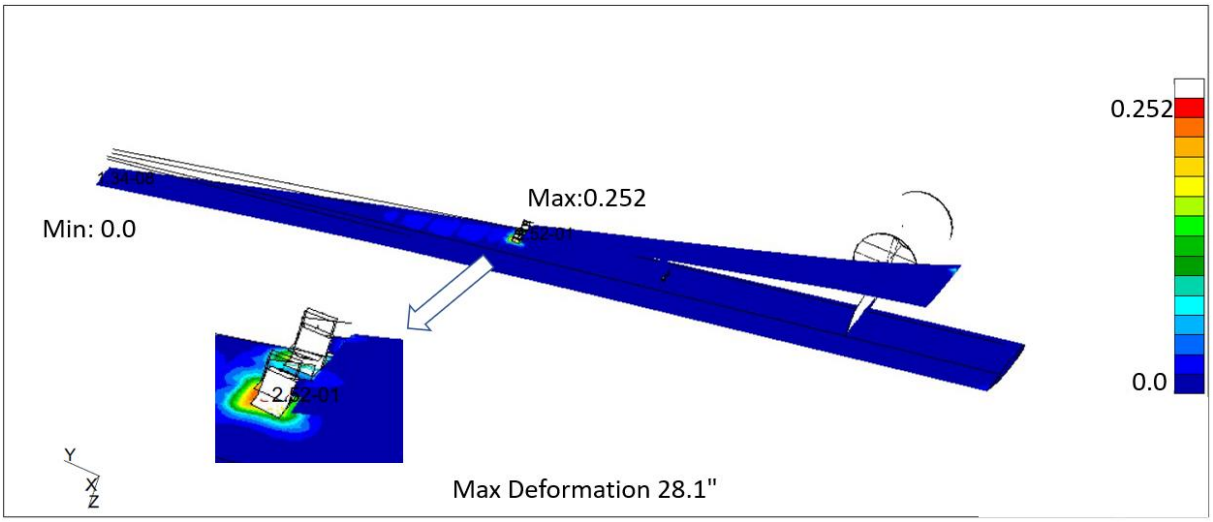

Figure 12. Unreinforced global TTBW FEM displacements and Tsai-Hill Failure Index results.

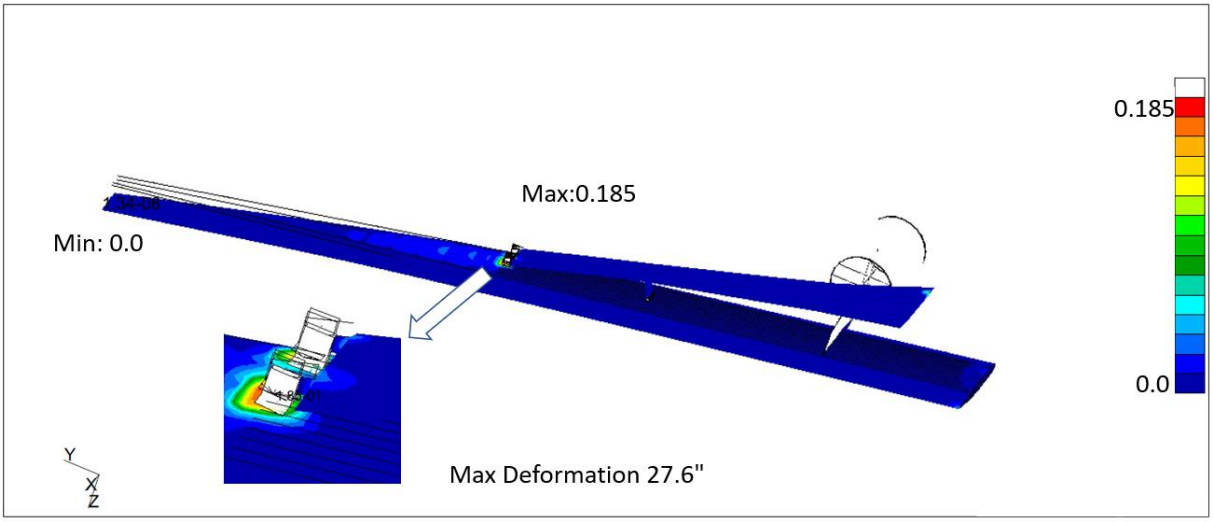

Figure 13. Beam-reinforced global TTBW FEM displacements and Tsai-Hill Failure Index results.

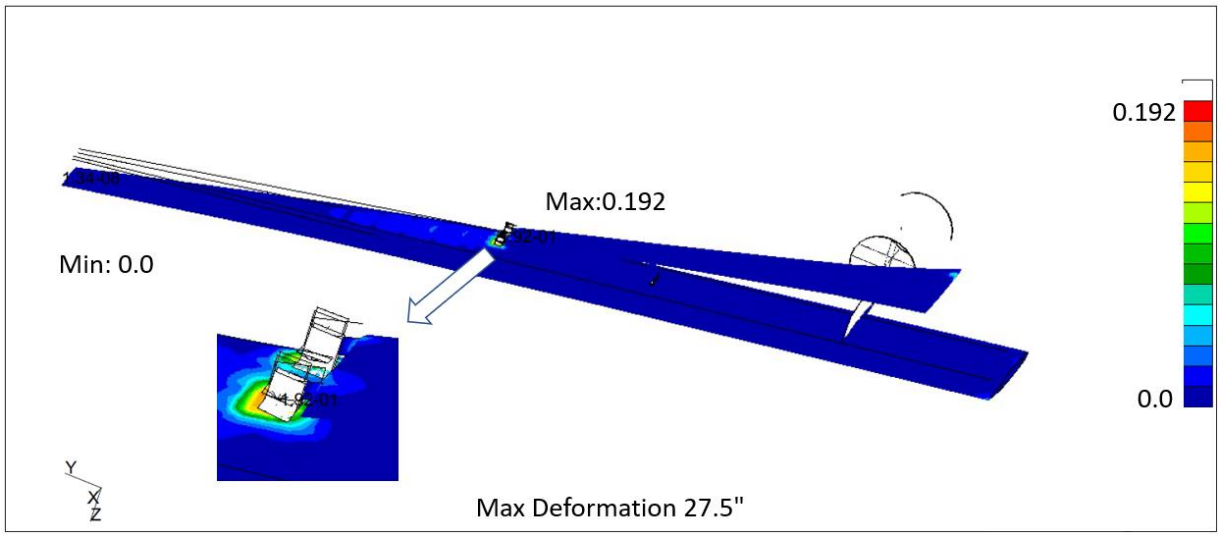

Figure 14. CSL-reinforced global TTBW FEM displacements and Tsai-Hill Failure Index results.

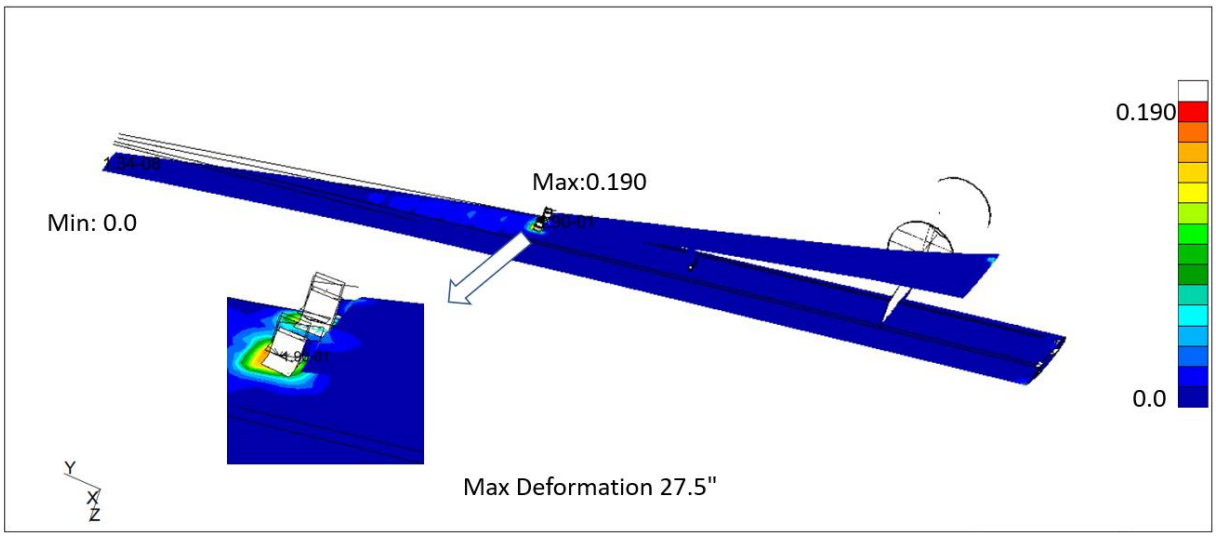

Figure 15. Hybrid-reinforced global TTBW FEM displacements and Tsai-Hill Failure Index results.

Displacements for both the CSL approach and the hybrid approach are within 1% of the beam-reinforced baseline results, with the hybrid approach resulting in a slightly stiffer model than the CSL approach. The failure indices only match to within 4% for both models. Given the close correlation to the beam-reinforced baseline for both example cases, either approach may be considered a candidate for use in global sizing efforts, though the improvement in failure index agreement may make the hybrid approach more desirable.

V. Structural Sizing Approach

With future alternate design and modeling approaches in mind, an initial structural sizing was still required to begin the development of a global FEM of the TTBW. The LS-OPT software framework [10] was selected as a design optimization tool to size the shell thicknesses in the MSC NASTRAN FEM. The LS-OPT software can be set up to run any command-line driven analysis code, such as a Python script or a FE analysis code. The LS-OPT software can be used to perform an optimization on a response surface representing the selected objective as a function of the design variables, or the software can be used to perform optimization using direct simulation with a genetic algorithm. Due to errors between the response surfaces and the actual simulated values observed in early stages of this study, direct simulation with a genetic algorithm was selected.

For the initial sizing study, the design variables were the ply thicknesses for the symmetric composite laminate representing the wing and struts. For each composite laminate, variables were used to define the number of plies for each orientation angle used in the laminate: 0^o, 45^o, and 90^o, using variables n0, n45, and n90, respectively. Quasi-isotropic ([45/-45/0/90]) stacks of plies were used as outer plies in each laminate. The number of stacks was the minimum value of n0, n45, and n90 associated with the laminate. The remaining plies (the difference between the minimum and n0, n45, and n90) were placed as innermost plies in the laminate. For each bay in the global FEM, separate composite layups were used for the bay covers (upper and lower), the spars, and the ribs. For the wing and struts, the total number of bays was 51, corresponding to a total of 53 ribs. Each bay had two property sets (one for the spars and one for both sets of covers) and each rib had one property set, for a total of 155 property sets. The three variables, n0, n45, and n90, were assigned per composite laminate, bringing the total number of design variables to 465.

A Python script was developed to map the array of design variables to NASTRAN PCOMP property sets. This Python script was designed to reduce the number of required input variables by linearly interpolating ply thicknesses between user defined locations (referred to as “control points” in the remainder of this discussion) with known total laminate thicknesses. On the wing, eight control points were used for the covers, one was used for the spars, and one was used for the ribs. In the main strut, five control points were used for the covers, three were used for the spars, and three were used for the ribs. With a total of 21 control points, the number of design variables was reduced to 63. The wing cover control points are shown in Figure 16 to illustrate one configuration of thse points. The remaining control points are removed for clarity.The remainder of the original design variables were assigned to specific laminate regions between their closest control points. Their values were then determined as a linearly scaled percentage of the nearest control points based on their proximity to said control points.

LS-OPT was used to determine the minimum structural weight of the wing, subject to buckling and strength constraints under the +2.5-g climb and -1-g down gust loading discussed in Section II, with an applied factor of safety of 1.5. Two sizing optimizations were conducted using IM7/8552 composite properties, and the Tsai-Hill criteria as a strength constraint. In one sizing study, the laminate was unstiffened. In the other study, CSL-reinforced laminates, as discussed in Section IV, were used in the wing and main strut covers. Blade stiffeners that were 2-in. high, and 0.2-in. thick made of quasi-isotropic IM7/8552 with a 5-in. spacing were assumed and not optimized). In Figure 17, the panel thickness in the wing and main strut components are plotted against the spanwise bay location.

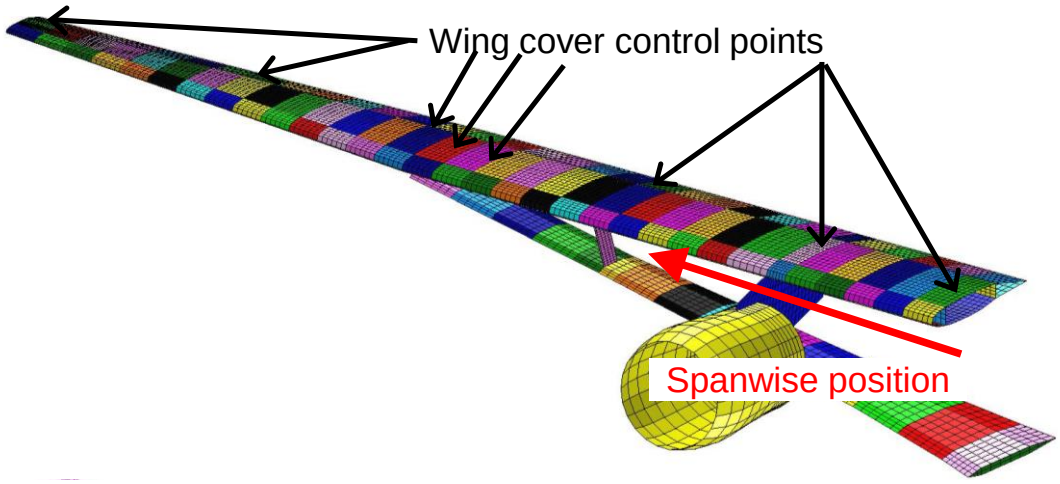

Figure 16. Thickness control points on FEM.

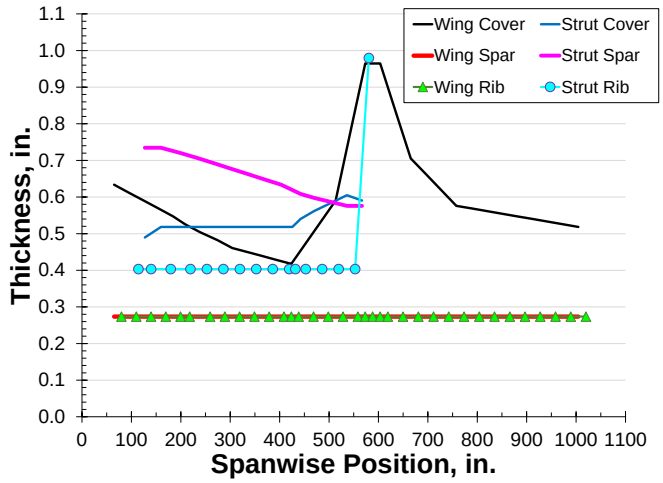

(a) Unstiffened composite design

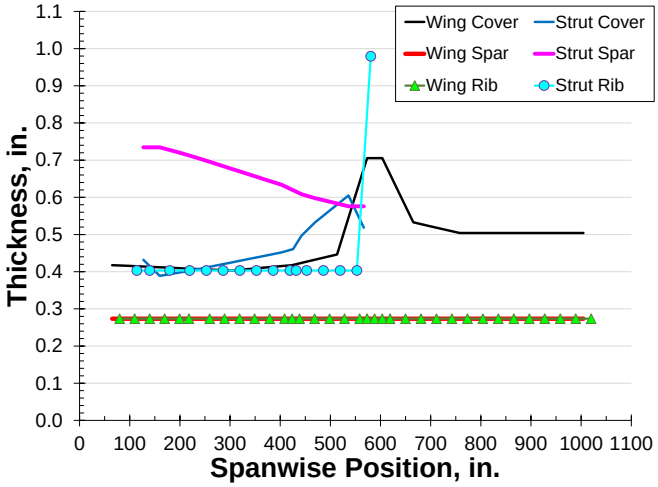

(b) CSL-reinforced composite design

Figure 17. Thickness variation with spanwise position (from root to tip).

The optimum weight for the CSL-reinforced composite design was 19.7% lower than for the unstiffened composite design. In comparing the plots of Wing Cover thickness in Figure 17a and 17b, it is seen that the largest reduction in thickness is possible for this component at the mid-span position. Smaller reductions occur over the span for the strut covers. This reduction is the expected difference in behavior between an unstiffened model and a stiffened model. The critical constraint in the optimization was the minimum eigenvalue for buckling due to the +2.5-g climb load case (as shown in Figure 18), and the Tsai-Hill failure index from a static analysis at the same +2.5-g climb load case. Both critical constraints had an applied factor of safety of 1.5.

An alternative to mechanically fastened blade stiffeners common in composite aircraft is composite-only integral stiffening. Before attempting to represent integral stiffeners in the numerical models, a study of manufacturing and design issues related to integral stiffening was conducted and is discussed in section VI.

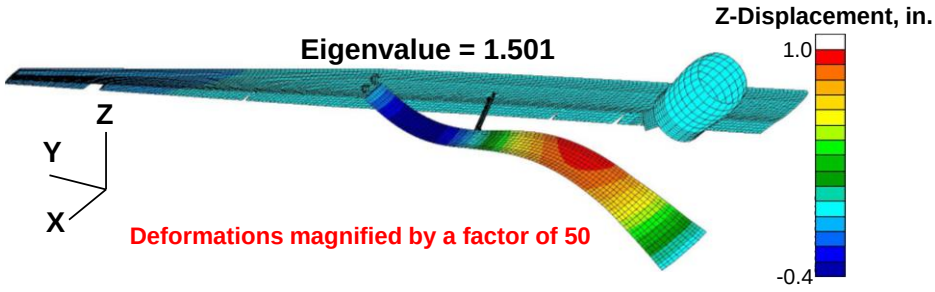

Figure 18. Mode shape of CSL-reinforced global TTBW FEM at lowest eigenvalue for 2.5-g load.

VI. Integrally Stiffened Panel Design and Manufacturing Approach

A design opportunity for the TTBW is the use of integrally stiffened panel sections for either the wing or the main strut. These panels would replace the traditional skin-stringer panels, which use stiffeners riveted or bonded to the skin surface, with lighter panels constructed with integral stiffeners. Before integrally stiffened composite panels can be analyzed as part of the sizing and optimization process, manufacturability of these panels should be considered and understanding of their behaviors under load should be explored.

Designs using integral stiffeners and tow steering were developed to be representative of portions of wing covers for a traditional wing (not a TTBW) [11]. Tows are strips of material placed along a programmed straight or curved path during the automated fiber placement (AFP) process. AFP is a common manufacturing method used for aerospace structures. During this previous design study, panels were assumed to be contained within an area between ribs and spars, resulting in designs of panels small enough to build and test. This investigation showed improved strength in comparison to straight fiber panels, while simultaneously reducing weight. Limited testing was conducted to explore manufacturing options and validate the design methodology. Panels representative of the most lightly loaded regions (those at the wing tip) were fabricated using AFP where integral stiffeners were created by overlapping tows and tested using boundary conditions to simulate rib and spar locations.

To continue this study, an investigation [12] was performed to determine manufacturing limitations on integral stiffening design and fabrication of panels. These integral stiffeners could replace or reduce the number of traditional stiffeners while removing the need for fasteners and allow for larger rib spacing compared to traditional designs. For this comparison to be valid, these lighter panels would not be restricted to the same dimensions but would include integral stiffeners at spar and rib locations. However, rather than go to a final design in the first fabrication attempt, progressively complex stiffener patterns were considered. Panel designs were first considered with relatively tall orthogonal composite stiffeners. To simulate this construction method, the first manufacturing trials consisted of a skin layer with composite stiffeners placed on the skin surface via AFP, as shown in Figure 19. However, this design was simply a starting point to develop a manufacturing baseline since these stiffeners are not integral and could separate from the skin easily, requiring fasteners to join them to the skin, thus reducing any benefit.

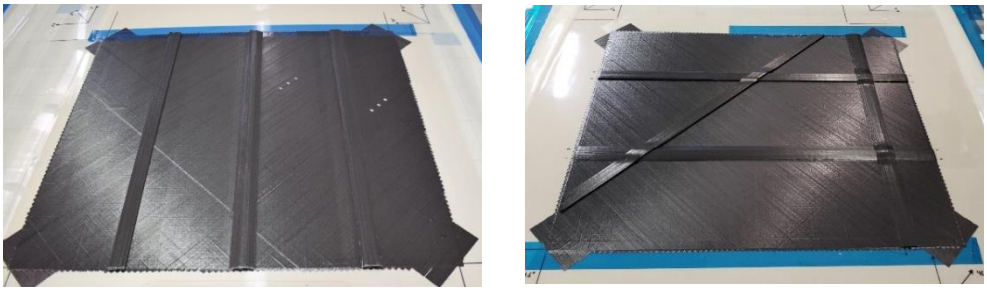

Figure 19. Stiffened panels containing only composite material.

As an alternative to adding stiffeners to the surface of a completed skin, the integral-stiffening approach was examined. For integral stiffeners, the stiffener plies were interleaved between the skin layers. Multiple integral-stiffener configurations were manufactured, some of which are shown in Figure 20, and the remainder of which are contained in Ref. [11]. Simple stiffener intersection configurations were manufactured initially, as shown in Figures 20a and 20b. However, in Figures 20c and 20d, examples of the more complex stiffener investigations are shown. In Figure 20c, there are two arced stiffeners as a lead-in towards further tow-steered stiffener concepts.

In addition to stiffener angle and configuration changes, alternate material forms were considered. Thin ply material, typically classified as material that is between 0.003 in. and 0.005 in. thick, was used for its additional strength benefits and weight savings, as indicated by prior experimental and analytical results [13]. A hybrid panel with thin-ply material used for the stiffeners and the standard-thickness material (0.0085 in. thick, in this case) used for the skin plies is shown in Figure 20d. Post-cure nondestructive evaluation and testing of these panels has not yet been conducted. Feedback from that work will guide further design and manufacturing studies.

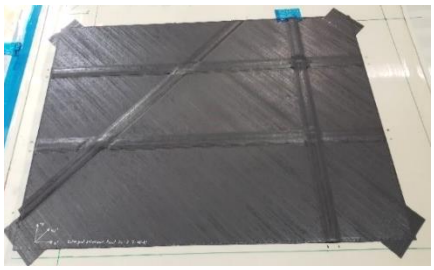

(a) Orthogonal stiffeners replicating traditional spars and ribs (b) Stiffener angle investigation

(c) Arced stiffener investigation (d) Material investigation.

Figure 20. Stiffened panels with interleaved stiffeners between skin plies.

The primary goal of the integral-stiffener development effort described is to establish machine limitations and determine buildable, structurally efficient designs for integral-stiffener geometry. The overarching goal of the integral-stiffener project is to develop methods to reduce aircraft weight, and to achieve more fuel-efficient designs, just as with developing the structural sizing methods presented earlier within this paper.

VII. Concluding Remarks and Forward Work

A composite smeared layer (CSL) stiffener modeling approach proposed in this paper appears to be a viable method of modeling stiffened panels as an alternative to modeling individual stiffeners. This method was successfully employed in the global FEM of a transonic truss-braced wing (TTBW) aircraft and integrated into the global model used for optimization. The smeared approach resulted in maximum displacements within 1% of the results for the model containing beam stiffeners. The LS-OPT design tool was used to optimize sizing for the wing and strut models using the CSL approach. Integrally stiffened panel explorations will continue to lead to further design iterations which minimize weight while maintaining or increasing strength when compared to traditionally stiffened panels,

VIII. References

[1] Droney, C. K., Sclafani, A. J., Harrison, N. A., Grasch, A. D., and Beyar, M. D., "Subsonic Ultra Green Aircraft Research: Phase III – Mach 0.75 Transonic Truss-Braced Wing Design," NASA/CR–20205005698, September 2020.

[2] Harrison, N. A., Gatlin, G. M., Viken, S. A., Bevar, M., Dickey, E. D., Hoffman, K., and Reichenbach, E. Y., "Development of an Efficient M=0.80 Transonic Truss-Braced Wing Aircraft," AIAA 2020-0011, AIAA SciTech 2020 Forum, Orlando, FL, January 6-10, 2020

[3] Maldonado, D., Viken, S. A., Housman, J. A., Hunter, C. A., Duensing, J. C., Frink, N. T., Jensen, J. C., McMillin, S. N., and Kiris, C. C., "Computational Simulations of a Mach 0.745 Transonic Truss-Braced Wing Design," AIAA 2020-1649, AIAA SciTech 2020 Forum, Orlando, FL, January 6-10, 2020.
[4] Fugate, J., Nguyen, N. T., and Xiong, J., "Aero-Structural Modeling of the Truss-Braced Wing Aircraft Using Potential Method with Correction Methods for Transonic Viscous Flow and Wing-Strut Interference Aerodynamics," AIAA 2019-3028, AIAA Aviation 2019 Forum, Dallas, TX, June 17-21, 2019.
[5] Gur, O., Bhatia, M., Schetz, J.A., Mason, W. H., Kapania, R. K., and Mavris, D. N., "Design Optimization of a Truss-Braced Wing Transonic Transport Aircraft," *Journal of Aircraft*, Vol. 47, No. 6, 2010.
[6] Mason, B. H. and Quinlan, J. R., "Conceptual Design Shop: A Tool for Rapid Airframe Structural Modeling," AIAA 2018-2001, AIAA SciTech 2018 Forum, Kissimmee, FL, January 8-12, 2018.
[7] PATRAN 2016 Release Guide, MSC Software, MSC Software, Santa Ana, CA 92707.
[8] Anonymous, *NASTRAN Analysis Quick Reference Manual*, MSC Software, Santa Ana, CA.
[9] Zahn, A., and Lovejoy, A. E., "Test and Analysis Correlation of Standard and Hybrid Standard/Thin-ply Composite Notched Test Specimens," AIAA SciTech 2020 Forum, AIAA Paper 2020-0478, Orlando, FL, January 6 – 10, 2020.
[10] Stander, N., Eggleston, T., Craig, K., and Roux, W., "LS-OPT User's Manual A Design Optimization and Probabilistic Analysis Tool for the Engineering Analyst," Version 2, Oct. 2003.
[11] Tatting, B. F., "Tow-Steered Panels for Tailored Wings," Final report for NASA Contract 80LARC18F0105, Task 601030USC, T18-601030-USC, June 2019.
[12] Cardona, A. M., Jegley, D. C., and Lovejoy, A. E., "Manufacturing Trials of Integrally Stiffened Panels for Flight Applications," AIAA SciTech 2023 Forum, National Harbor, MD, January 23-27, 2023.
[13] Zahn, A. M., "Finite Element Analysis Investigation of Hybrid Thin-Ply Composites for Improved Performance of Aerospace Structures," Master's Thesis, Old Dominion University, 2020.